University of Pennsylvania

School of Engineering and Applied Science

Department of Electrical and Systems Engineering

ESE 3190 — Spring 2025

Fundamentals of Solid-State Circuits

Final Project

Metal Detector

Hesham Nabil Hosny Maher

58309713

Submission Date: Friday, Apr 25, 2025

Contents

Introduction

Metal detectors are instruments designed to detect the presence of metallic objects by sensing the disturbance they cause to electromagnetic fields. They find applications in diverse fields such as security screening, archaeology, treasure hunting, and industrial inspections. In the context of this project, a metal detector was constructed using fundamental solid-state circuit components, emphasizing oscillator design, frequency mixing, amplification, and signal processing.

Operating Principle

The fundamental operating principle of a metal detector relies on the interaction between a time-varying magnetic field and a conductive object. When an alternating current (AC) passes through a coil (inductor), it generates a time-varying magnetic field according to Faraday's Law of Electromagnetic Induction. When a metallic object enters this magnetic field, eddy currents are induced within the object. According to Lenz's Law, these eddy currents generate a secondary magnetic field that opposes the original magnetic field, effectively altering the inductance of the coil.

This change in inductance can be exploited in different ways to detect the presence of metal. In this project, a frequency-based detection method was employed. Two oscillators are used: one with a fixed inductance (reference oscillator) and one with a custom-built air-core inductor (variable oscillator). Both oscillators are initially tuned to oscillate at the same frequency, ideally 50 kHz. The resonant frequency of each oscillator is determined by the LC (inductor-capacitor) resonance condition:

$$f_{\text{res}} = \frac{1}{2\pi\sqrt{LC}} \tag{1}$$

When a metallic object is brought near the variable inductor, the eddy currents induced in the metal reduce the effective inductance L of the coil. According to equation (1), a reduction in L leads to an increase in the resonant frequency f_{res}. As a result, the variable oscillator will oscillate at a slightly higher frequency than the reference oscillator.

The outputs of the two oscillators are fed into a mixer circuit. A mixer is a nonlinear device that produces outputs at the sum and difference frequencies of the two inputs. The key output we are interested in is the *difference frequency*:

$$f_{\text{out}} = |f_{\text{variable}} - f_{\text{fixed}}| \tag{2}$$

In the absence of nearby metal, both oscillators operate at the same frequency, and the mixer output is ideally a DC signal or very low-frequency noise. However, when a metal object is detected, the frequency shift in the variable oscillator results in a nonzero difference frequency, typically within the audio range (e.g., 1 kHz), which can be amplified and sent to a speaker for audible indication.

1 Design Strategy

The design of the metal detector is centered around frequency comparison between two LC oscillators. The fixed oscillator uses a shielded commercial inductor, while the variable oscillator is built with a custom-wound air-core inductor that acts as a sensor. The outputs of the two oscillators are processed by a mixer stage, followed by amplification and filtering to produce an audio signal that is audible through a speaker.

Figure 1 shows the overall block diagram of the system.

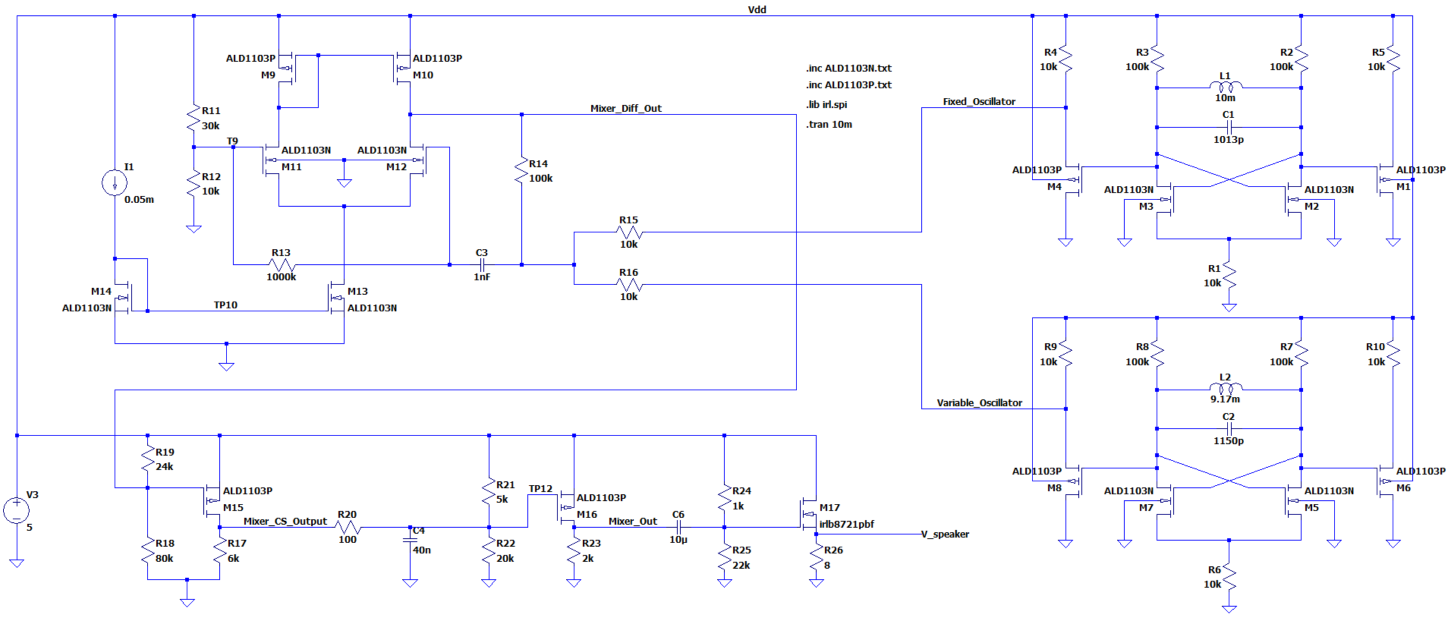

Figure 1: Circuit Schematic of the metal detector system.

The overall detection chain involves:

1. Generation of two close frequencies using LC oscillators.
2. Sensing the change in inductance due to eddy currents induced by nearby metal.
3. Mixing the oscillator outputs to detect the difference frequency.
4. Amplifying the difference signal for audible output through a speaker.

This method provides both detection and proximity sensing, as the magnitude of frequency shift depends on the size and distance of the metallic object relative to the inductor.

In addition to the fundamental oscillator and mixer circuits, a cascade of amplification stages, including common-source (CS) amplifiers and source follower (common-drain) amplifiers, are employed to ensure sufficient signal strength to drive a standard $8\,\Omega$ speaker. A low-pass filter is also included after the mixer to suppress high-frequency components and isolate the desired audio frequency signal.

1.1 Oscillator Stages

Each oscillator is constructed using a pair of cross-coupled MOSFETs configured to provide positive feedback. The LC tank in each oscillator determines its frequency. The fixed oscillator is tuned to 50 kHz using a 10 mH inductor and appropriate capacitors. The variable oscillator is similarly tuned but can shift slightly in frequency depending on nearby metal due to changes in inductance.

Images 2 and 3 show real oscilloscope outputs of the fixed and variable oscillators, respectively.

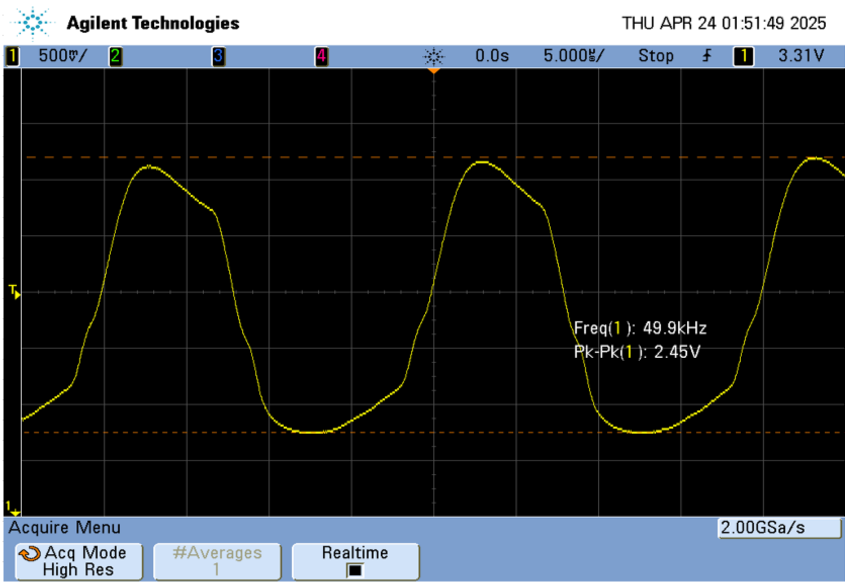

Figure 2: Oscilloscope capture of the fixed oscillator output at 49.9 kHz.

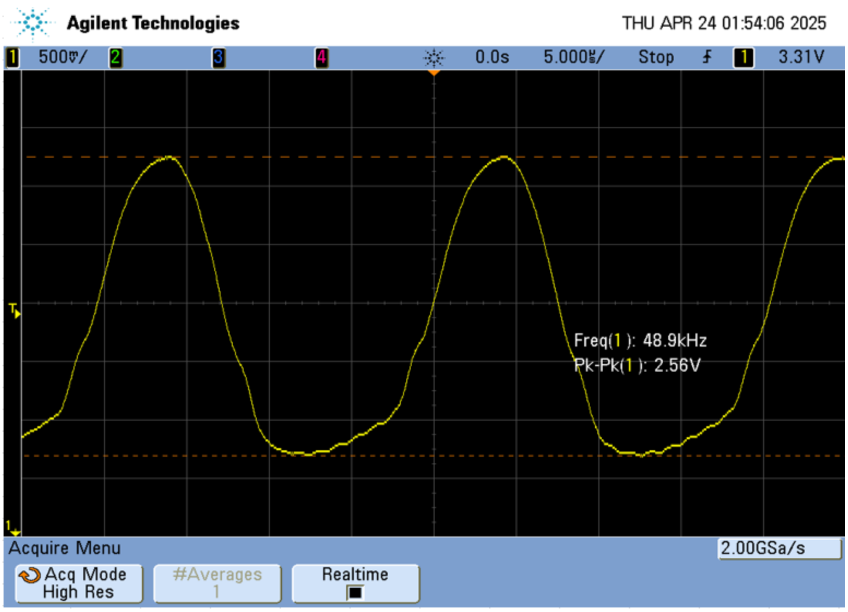

Figure 3: Oscilloscope capture of the variable oscillator output at 48.9 kHz.

1.2 Mixer Stage

The mixer receives inputs from both oscillators and outputs their difference frequency. The circuit uses a pair of differential amplifiers implemented using ALD1103 CMOS quad transistor arrays. The mixer produces a high-frequency signal modulated by the difference frequency.

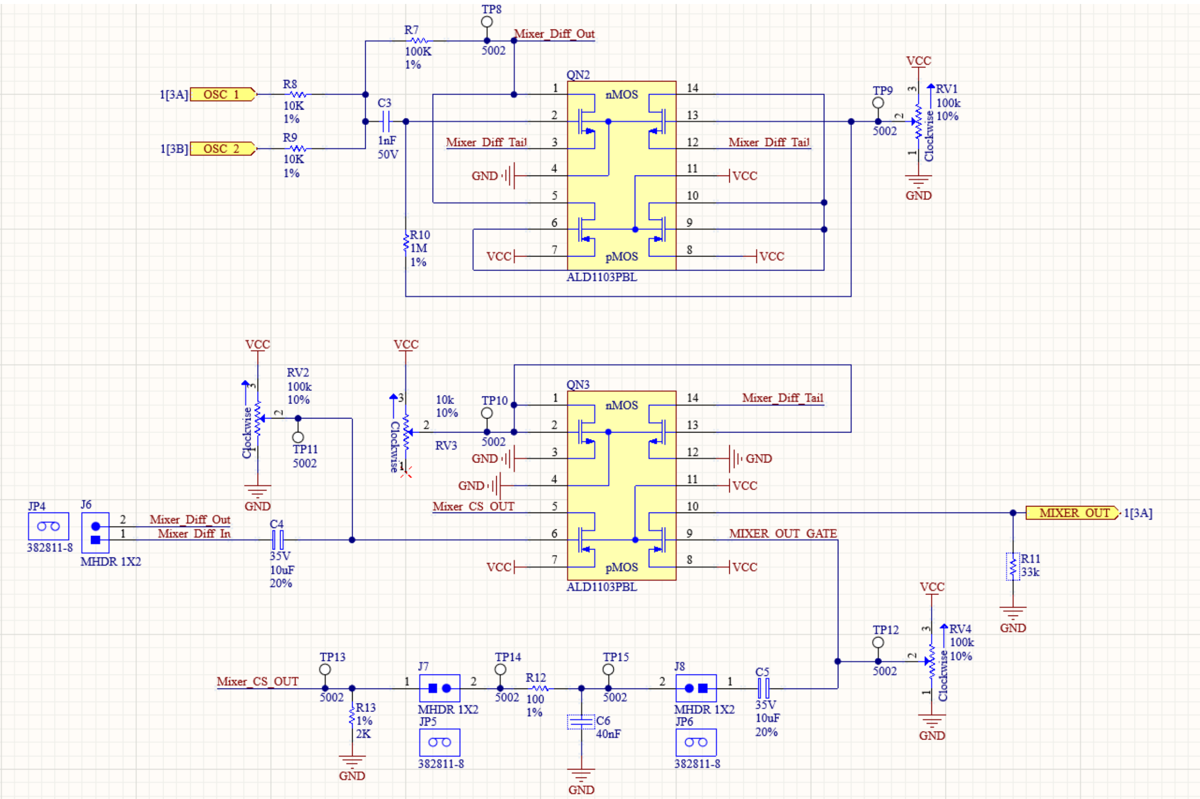

Figure 4: Mixer and amplification stage schematic.

1.3 Amplification and Filtering

The difference frequency produced by the mixer is passed through common-source and source-follower amplifiers to provide gain and proper drive strength. A low-pass filter removes high-frequency noise and isolates the audio tone.

Output Stage

The amplified audio signal is used to drive a small speaker. The speaker produces an audible tone whose frequency corresponds to the difference between the oscillators. This allows the user to hear changes in proximity or size of nearby metallic objects.

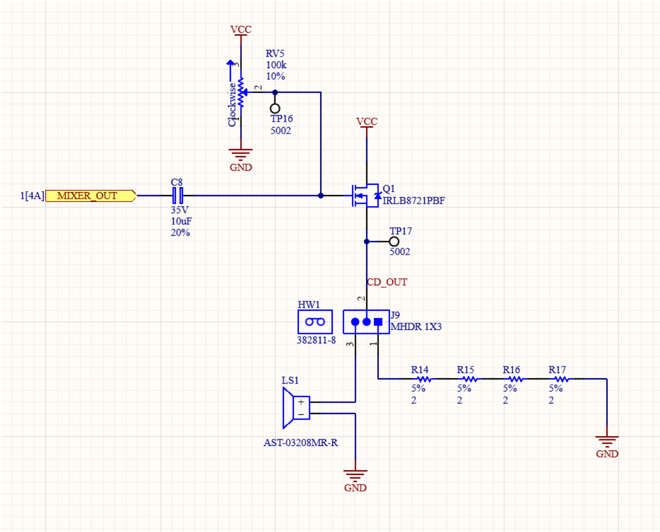

Figure 5: Schematic of the final output stage.

1.4 Full PCB Assembly

The final PCB integrates all stages and provides connection points for the custom inductor, USB power, speaker, and debugging test points.

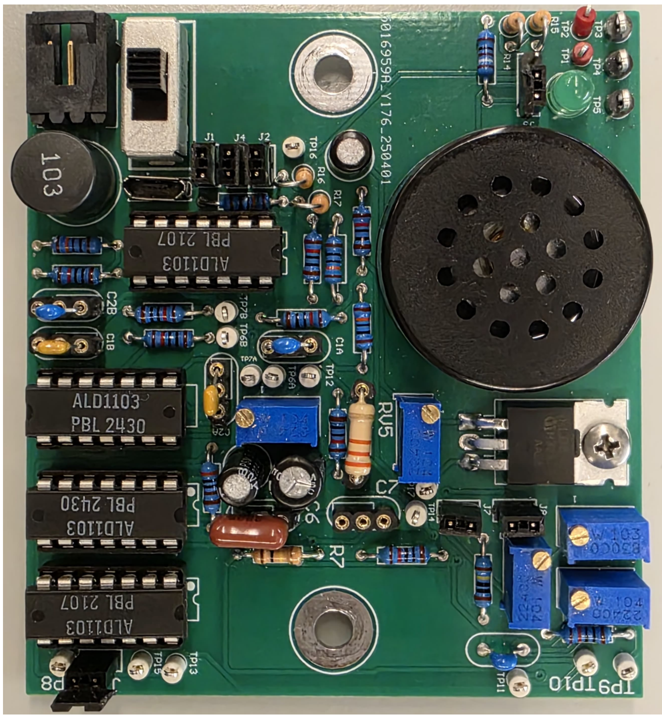

Figure 6: Fully assembled PCB with all components.

2 Hand Calculations

For the metal detector circuit to function correctly, each major design block must be carefully hand-calculated to ensure all transistors operate in their proper regions, oscillators resonate at desired frequencies, and amplifiers provide sufficient gain without distortion. Although some tolerances exist due to component inaccuracies and real-world noise, a solid hand calculation establishes a reliable baseline for circuit operation.

2.1 Oscillator Frequency Design

The fixed and variable oscillators are cross-coupled MOSFET circuits using LC tank resonators. The resonant frequency of an LC tank is given by:

$$f_0 = \frac{1}{2\pi\sqrt{LC}} \tag{3}$$

For the fixed oscillator:

- $L_{\text{fixed}} = 10\,\text{mH}$
- $C_{\text{fixed}} = 1.013\,\text{nF}$

Thus:

$$f_{\text{fixed}} = \frac{1}{2\pi\sqrt{10 \times 10^{-3} \times 1.013 \times 10^{-9}}} \approx 50\,\text{kHz} \tag{4}$$

For the variable oscillator:

- $L_{\text{variable}} = 9.17\,\text{mH}$
- $C_{\text{variable}} = 1.150\,\text{nF}$

Thus:

$$f_{\text{variable}} = \frac{1}{2\pi\sqrt{9.17 \times 10^{-3} \times 1.150 \times 10^{-9}}} \approx 49\,\text{kHz} \tag{5}$$

Both oscillators are tuned to frequencies close enough to generate a low-frequency beat signal when metal is detected.

2.2 Mixer Current Mirror Biasing

The current mirror sets the tail current I_{SS} for the differential amplifier at the mixer stage. The bias voltage V_b for the mirror is derived from the resistor divider formed by $R11 = 30\,\text{k}\Omega$ and $R12 = 10\,\text{k}\Omega$.

Using voltage division:

$$V_b = V_{DD} \times \frac{R12}{R11 + R12} \tag{6}$$

Substituting values:

$$V_b = 5 \times \frac{10}{30 + 10} = 5 \times 0.25 = 1.25\,\text{V} \tag{7}$$

Current Mirror Sizing:
Using the saturation current equation for a MOSFET:

$$I_D = \frac{1}{2}K_n(V_{GS} - V_{th})^2 \tag{8}$$

Assuming:
- $K_n = 5\,\text{mA/V}^2$ - $V_{th} = 0.73\,\text{V}$ - Mirror input transistor is biased at $V_b = 1.25\,\text{V}$
Thus:

$$I_{\text{mirror}} = \frac{1}{2} \times 5 \times (1.25 - 0.73)^2 = \frac{1}{2} \times 5 \times (0.52)^2 \tag{9}$$

$$I_{\text{mirror}} = 0.5 \times 5 \times 0.2704 = 0.676\,\text{mA} \tag{10}$$

Thus, $I_{SS} = 0.676\,\text{mA}$ total tail current.

Each branch of the differential pair will ideally carry:

$$I_1 = I_2 = \frac{I_{SS}}{2} = 0.338\,\text{mA} \tag{11}$$

2.3 Differential Pair Biasing and Operation

To ensure the differential pair remains in saturation:

$$V_{DS} > V_{GS} - V_{th} \tag{12}$$

The overdrive voltage V_{OV} is:

$$V_{OV} = V_{GS} - V_{th} \tag{13}$$

From the mirror:

$$V_{GS} = V_{th} + \sqrt{\frac{2I_D}{K_n}} \tag{14}$$

Substituting:

$$V_{GS} = 0.73 + \sqrt{\frac{2 \times 0.338 \times 10^{-3}}{5 \times 10^{-3}}} \tag{15}$$

$$V_{GS} = 0.73 + \sqrt{0.1352} \approx 0.73 + 0.368 = 1.098\,\text{V} \tag{16}$$

Thus, the gates of the differential pair are at approximately $1.1\,\text{V}$.

2.4 Common-Source Amplifier Biasing

The CS amplifier is biased through a resistor divider formed by $R18 = 80\,\mathrm{k\Omega}$ and $R19 = 24\,\mathrm{k\Omega}$.

Using voltage division:

$$V_{G,CS} = V_{DD} \times \frac{R19}{R18 + R19} \tag{17}$$

Substituting:

$$V_{G,CS} = 5 \times \frac{24}{80 + 24} = 5 \times 0.23 \approx 1.15\,\mathrm{V} \tag{18}$$

Thus, the gate voltage is $1.15\,\mathrm{V}$.

Calculating drain current:

$$I_D = \frac{1}{2} K_n (V_{G,CS} - V_{th})^2 \tag{19}$$

Substituting:

$$I_D = 0.5 \times 5 \times (1.15 - 0.73)^2 = 0.5 \times 5 \times 0.1764 = 0.441\,\mathrm{mA} \tag{20}$$

Calculating small-signal transconductance g_m:

$$g_m = \frac{2I_D}{V_{GS} - V_{th}} \tag{21}$$

$$g_m = \frac{2 \times 0.441}{1.15 - 0.73} \approx 2.1\,\mathrm{mS} \tag{22}$$

Voltage gain A_v using $R_D = 2\,\mathrm{k\Omega}$:

$$A_v = -g_m R_D = -(2.1 \times 10^{-3}) \times 2000 = -4.2 \tag{23}$$

2.5 Low-Pass Filter Design

The low-pass filter formed by $R20 = 10\,\mathrm{k\Omega}$ and $C4 = 40\,\mathrm{nF}$ removes high-frequency components.

Cutoff frequency:

$$f_c = \frac{1}{2\pi RC} \tag{24}$$

Substituting:

$$f_c = \frac{1}{2\pi \times 10^3 \times 40 \times 10^{-9}} \approx 3979\,\mathrm{Hz} \tag{25}$$

This effectively attenuates unwanted high-frequency artifacts while preserving the beat frequency of interest (1 kHz).

3 Simulation Results

The functionality of each circuit block was first verified through LTspice simulations before hardware fabrication. The following subsections present the key simulation results.

3.1 Fixed Oscillator Output

The fixed oscillator was designed to operate at approximately 50 kHz. The LTspice simulation waveform is shown in Figure 7.

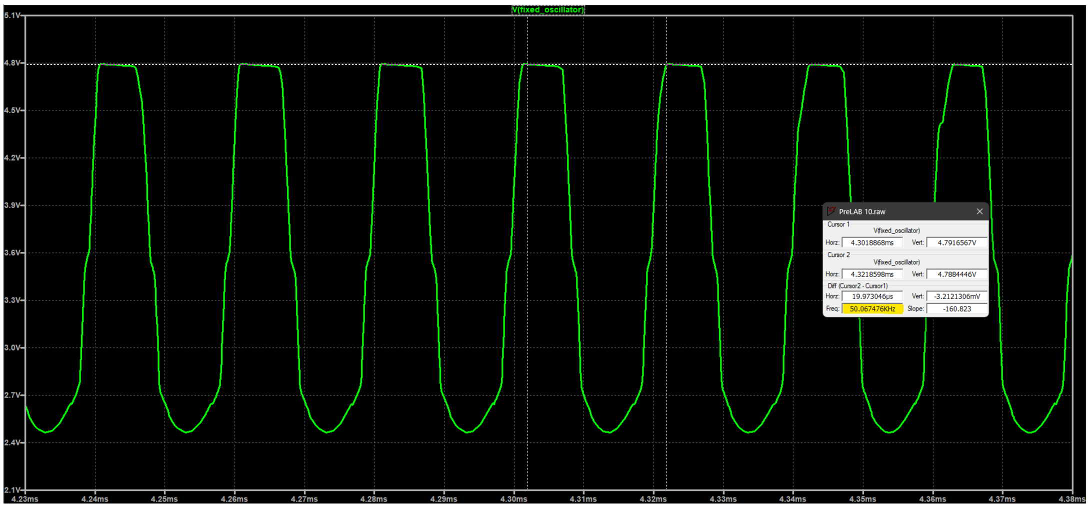

Figure 7: LTspice simulation output for the fixed oscillator.

The simulation confirms a clean periodic output at about 50 kHz, matching the design goal.

3.2 Variable Oscillator Output

Similarly, the variable oscillator was designed to operate close to 49 kHz. The simulated output is shown in Figure 8.

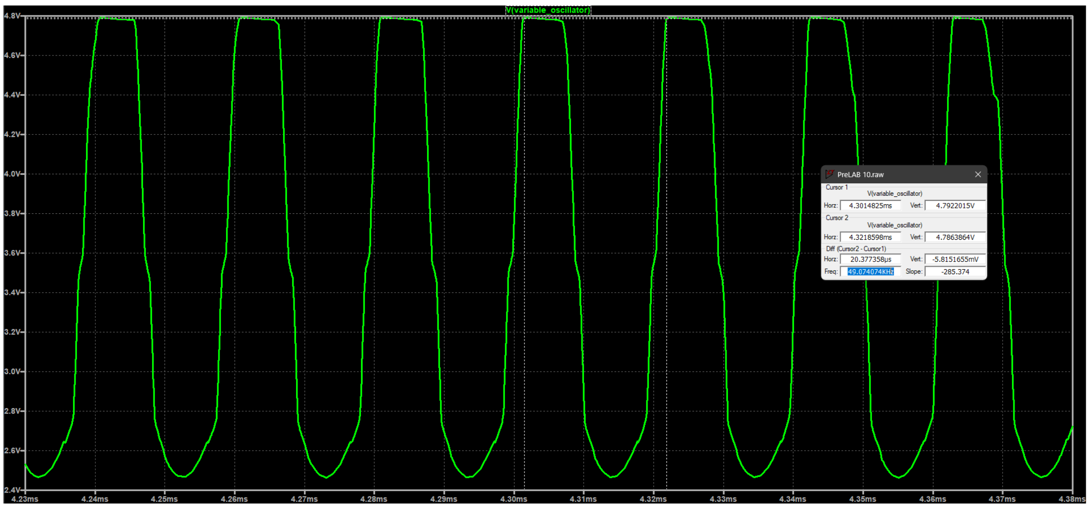

Figure 8: LTspice simulation output for the variable oscillator.

3.3 Mixer Stage Outputs

The outputs of the fixed and variable oscillators were fed into the mixer stage. Simulated differential and common-source outputs are shown below.

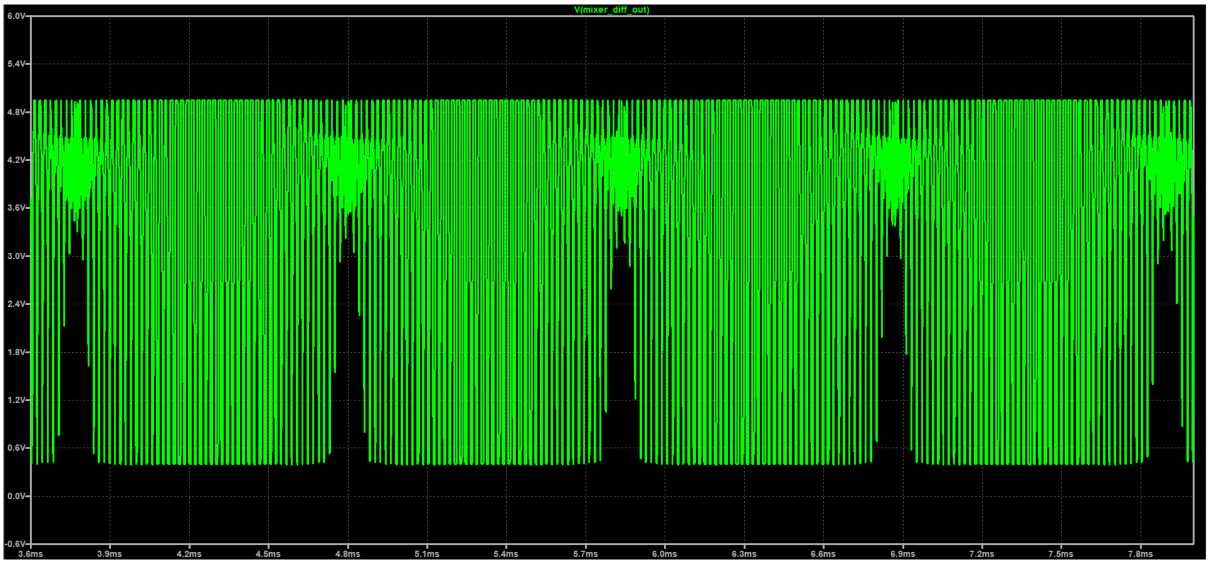

Figure 9: Differential output of the mixer (TP8) - simulation.

The mixer combines the outputs of the fixed and variable oscillators to produce both a differential and a common-source signal.

The differential output (TP8) primarily captures the frequency components resulting from the slight mismatch between the two oscillators, producing a beat frequency in the audio range (typically around 1 kHz).

Meanwhile, the common-source output (TP13) emphasizes the amplitude modulation caused by the frequency difference, showing clearer envelope variations that are easier to amplify and filter.

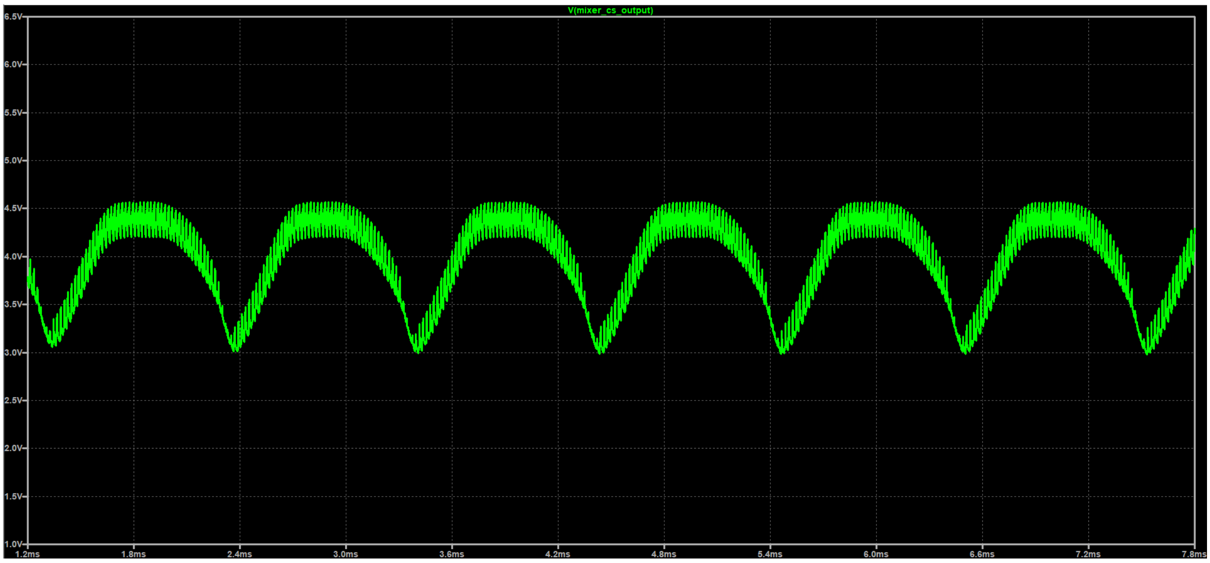

Figure 10: Common-source output of the mixer (TP13) - simulation.

3.4 Mixer Final Output

After amplification and low-pass filtering, the mixer output was observed. The simulated mixer output is shown in Figure 11.

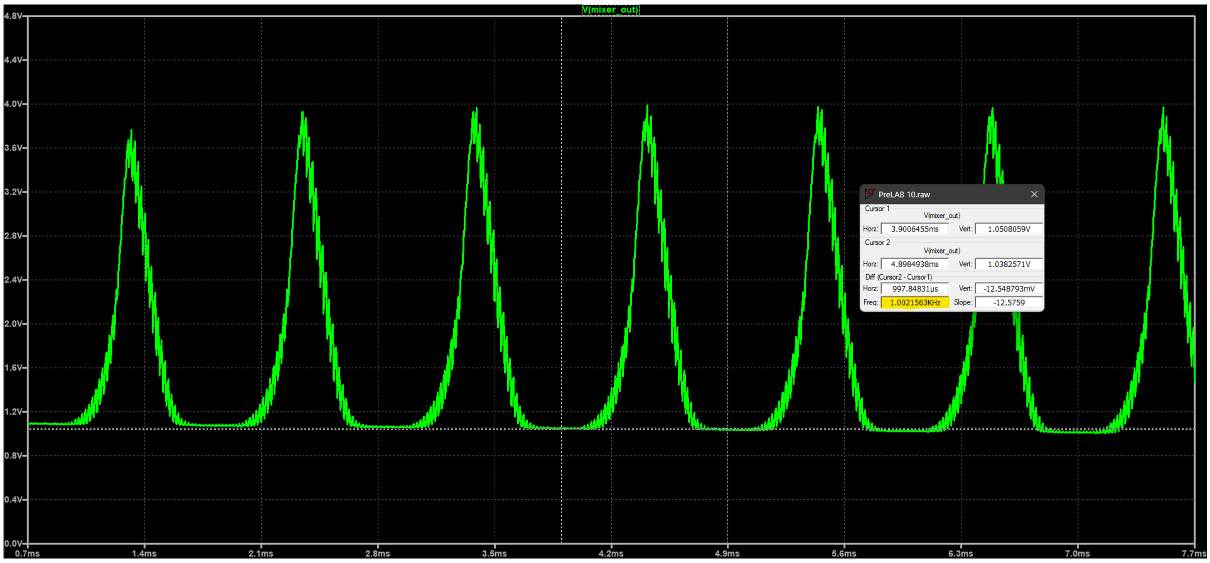

Figure 11: Mixer final output (TP16) FFT - simulation.

3.5 Speaker Output

Finally, the speaker output waveform after the driver stage was observed. Simulation output is shown in Figure 12.

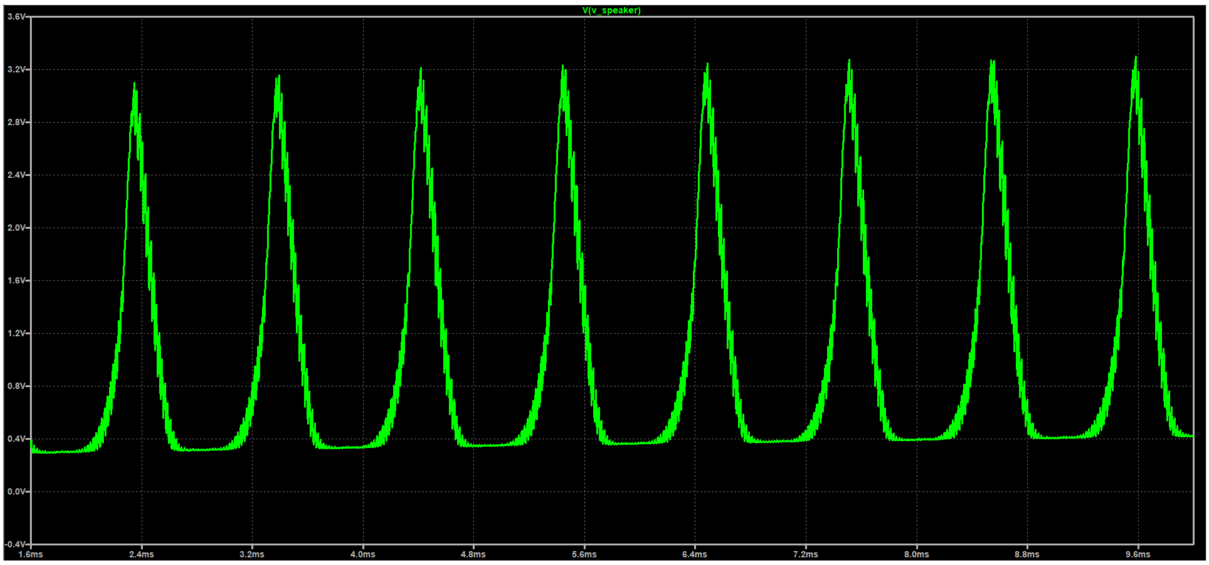

Figure 12: Simulated voltage across the speaker node (TP17).

These simulation results confirm that the circuit behaves as expected, with correct frequency difference detection by the mixer, and audible output generation.

4 PCB Layout

After verifying the functionality through simulations, the circuit was implemented in a printed circuit board (PCB) using Altium Designer. The PCB design integrates all major circuit blocks and pays close attention to layout practices such as ground planes, signal integrity, and component accessibility.

4.1 Full Layout Overview

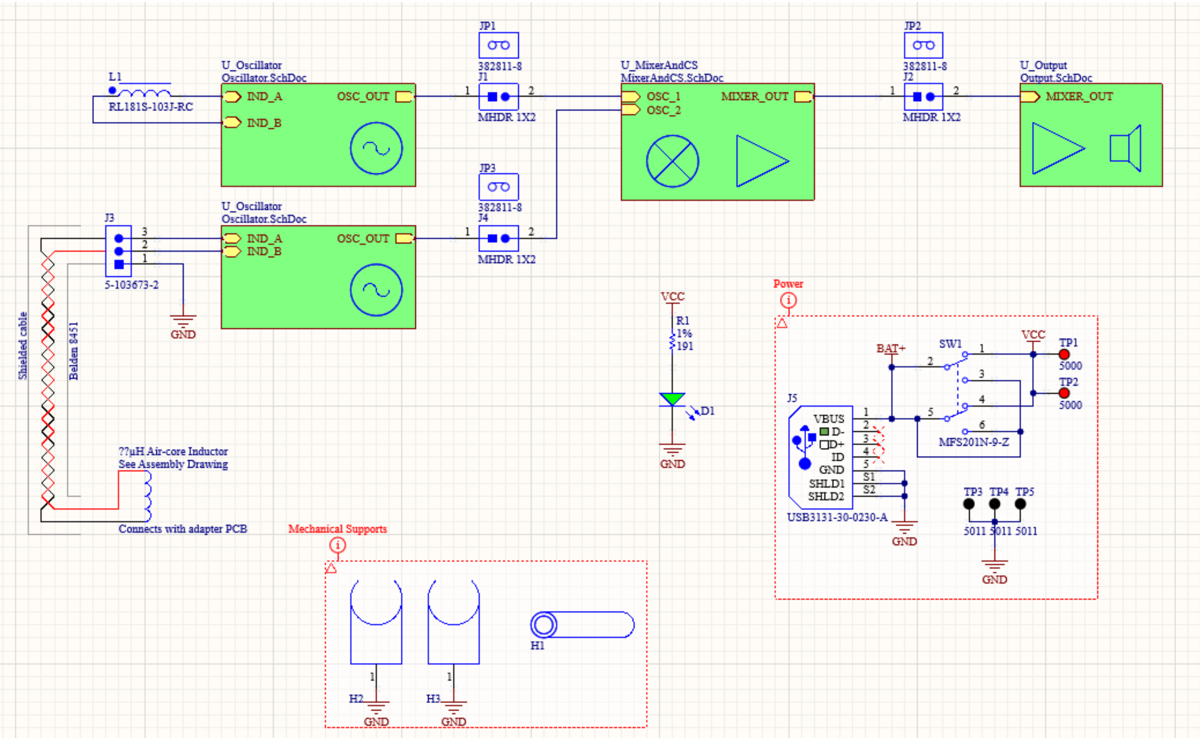

Figure 13: Top-level PCB layout overview including all major circuit sections.

The layout was divided logically as follows:

- **Top-left**: Fixed and variable oscillator circuits, generating the base frequencies.
- **Center**: Mixer stage combining oscillator outputs and producing the difference signal.
- **Middle-right**: Common-source amplifier stages boosting the beat frequency signal.
- **Bottom-right**: MOSFET output driver stage for driving the speaker.
- **Bottom-left**: Power management section and external connector interfaces.

4.2 Top Layer Routing

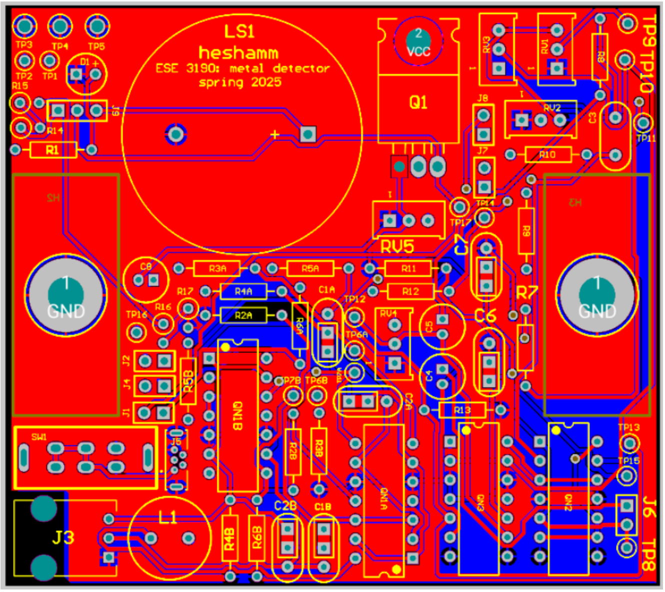

Figure 14: PCB Top Layer: highlighting signal traces and power routing.

The top layer (shown in red) primarily handles sensitive signal traces, short interconnections, and component placements for active circuitry.

4.3 Bottom Layer Routing

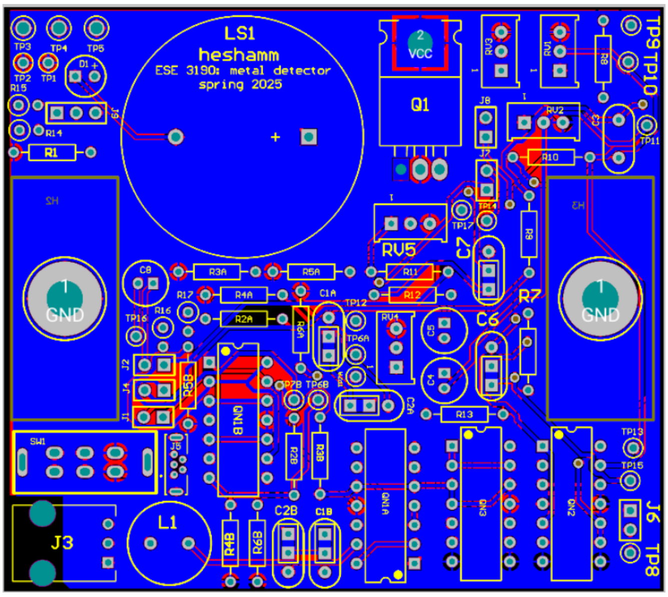

Figure 15: PCB Bottom Layer: ground planes and return paths.

The bottom layer (shown in blue) provides solid ground planes wherever possible to enhance noise immunity and to create low-impedance return paths for critical signals.

4.4 Assembled PCB

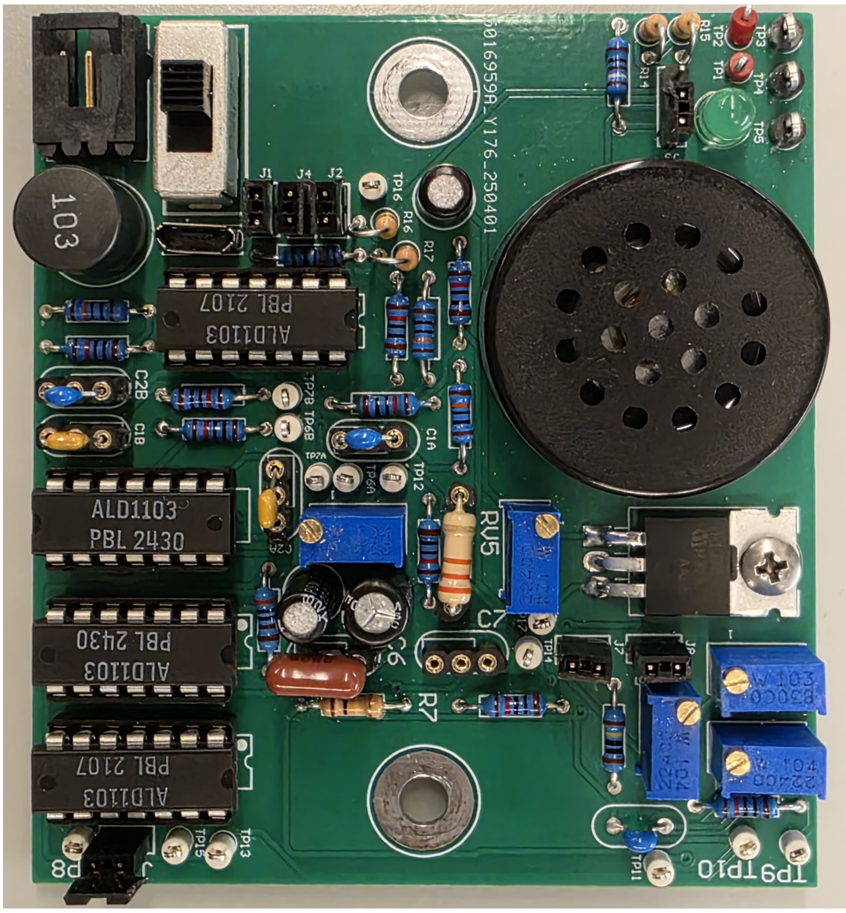

Figure 16: Fully assembled PCB with components soldered.

The completed board integrates all functional blocks and provides easy-to-access test points for debugging and measurements. The final assembly confirmed proper footprint design, mechanical alignment, and electrical connectivity across all stages.

5 Measurement Results

After assembling the PCB and biasing the circuits according to design expectations, measurements were collected using an oscilloscope to verify the operation of each major circuit stage. While slight differences between hand calculations, LTspice simulations, and hardware measurements are expected due to second-order effects, parasitics, and real-world component tolerances, the overall functionality and trends align closely with design goals. Minor adjustments were made to resistor and capacitor values on the real board to optimize practical performance.

5.1 Fixed Oscillator Output

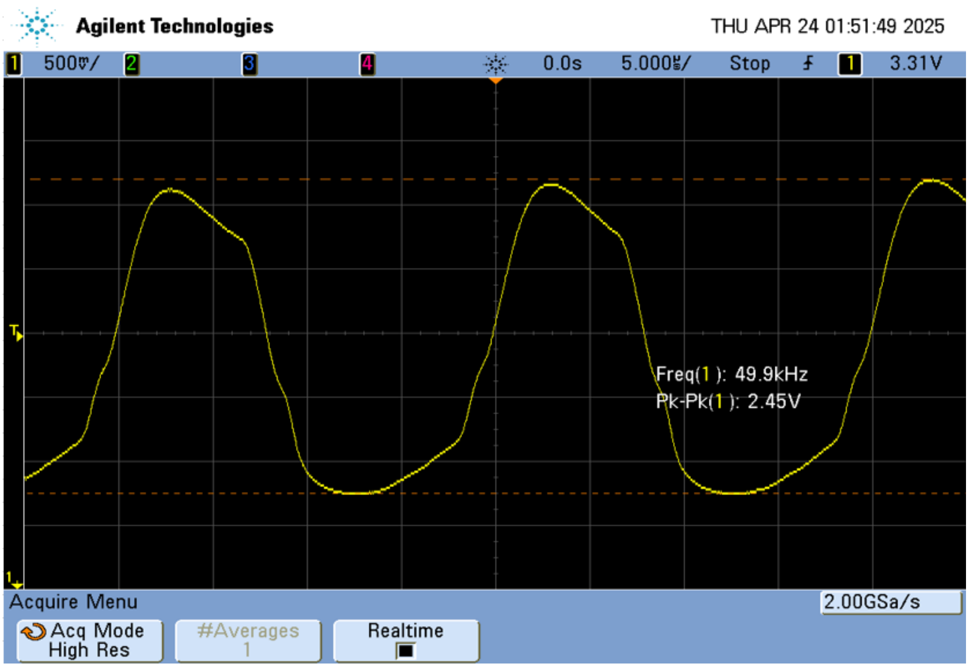

Figure 17: Measured output of the fixed oscillator (49.9 kHz).

The fixed oscillator output shows a clean periodic signal at approximately 50 kHz.

5.2 Variable Oscillator Output

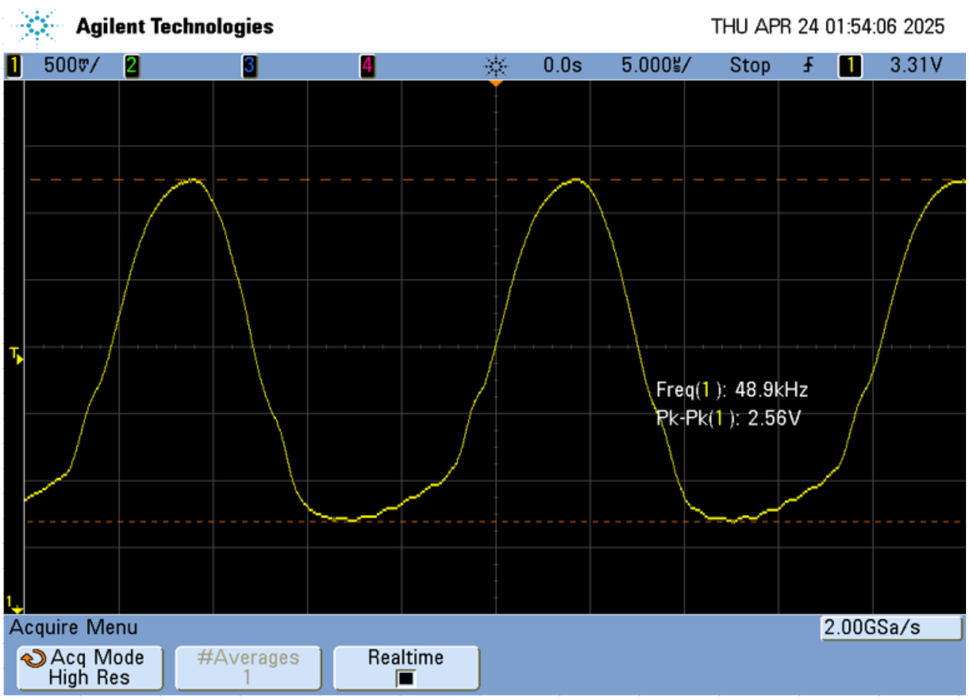

Figure 18: Measured output of the variable oscillator (48.9 kHz).

The variable oscillator outputs a waveform at approximately 49 kHz.

5.3 Mixer Stage Differential Output & FFT (TP8)

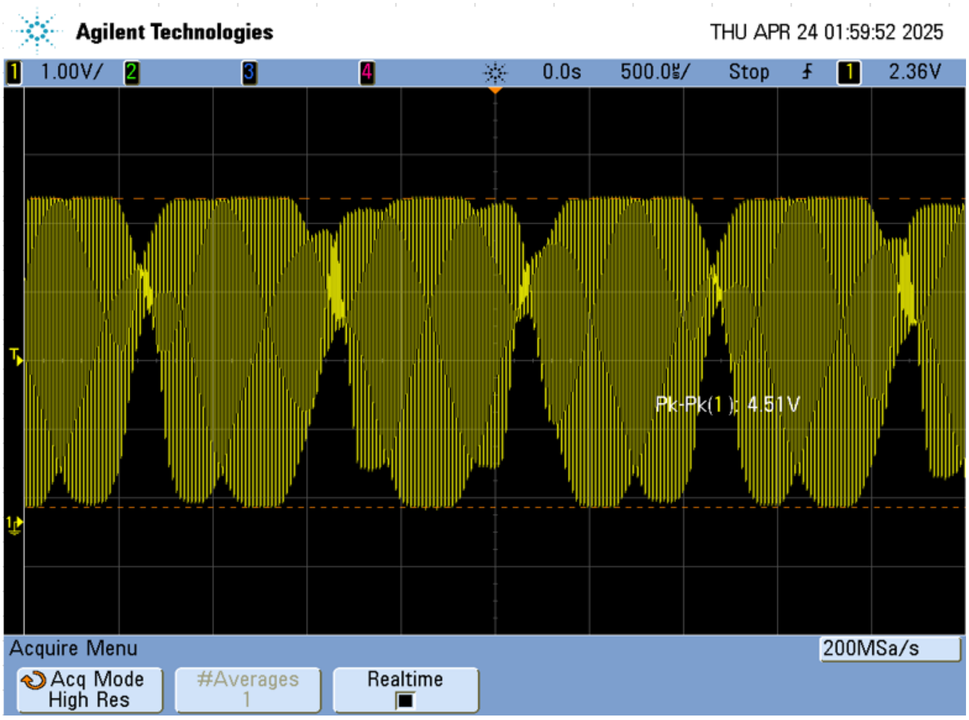

Figure 19: Measured differential output of the mixer (TP8).

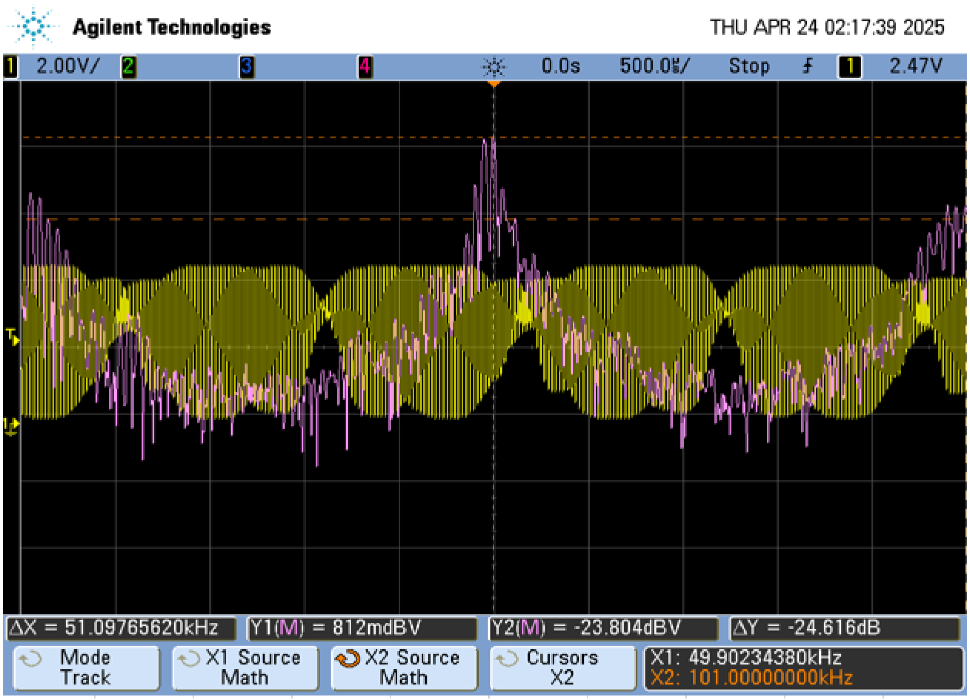

Figure 20: FFT of the differential output showing beat frequency components.

The FFT shows multiple frequency components present at the differential output of the mixer, which must be amplified and filtered to isolate the desired signal.

5.4 Mixer Stage Common-Source Output & FFT (TP13)

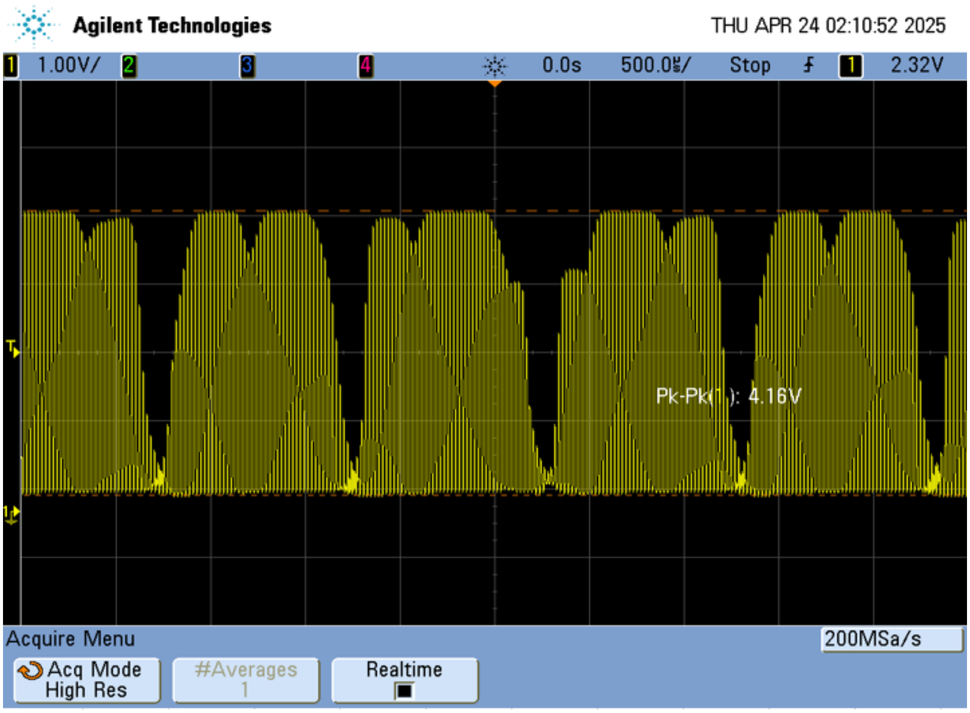

Figure 21: Measured common-source output of the mixer (TP13).

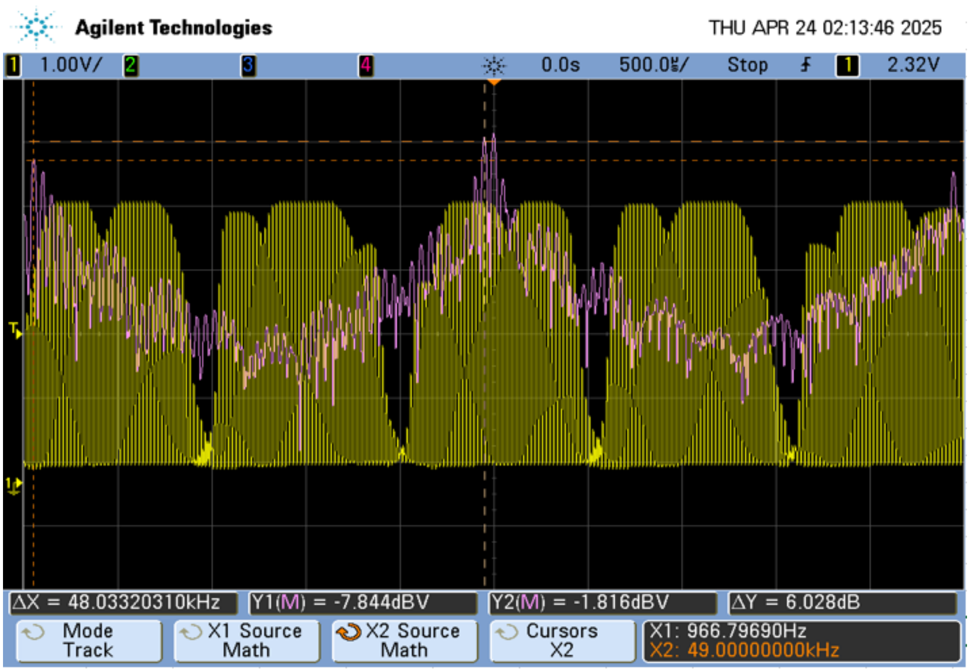

Figure 22: FFT of common-source output showing clear beat frequency.

After amplifying the signal, the high-frequency components are removed using a low-pass filter, followed by a second amplification stage.

5.5 Final Mixer Output After Filtering (TP16)

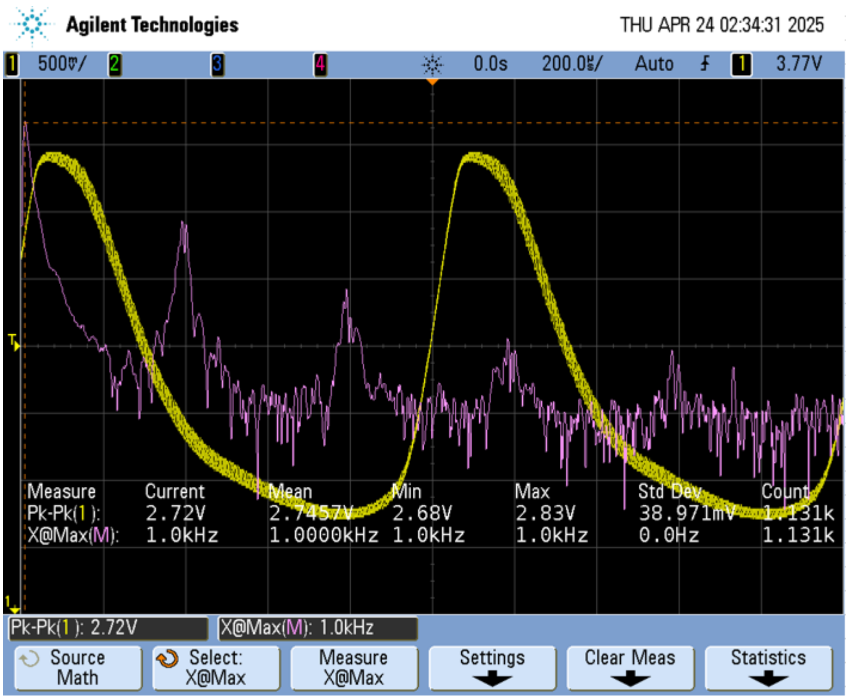

Figure 23: Filtered mixer output showing clean low-frequency tone (TP16).

After low-pass filtering, the output shows a sinewave at the difference frequency.

5.6 Speaker Output (TP17)

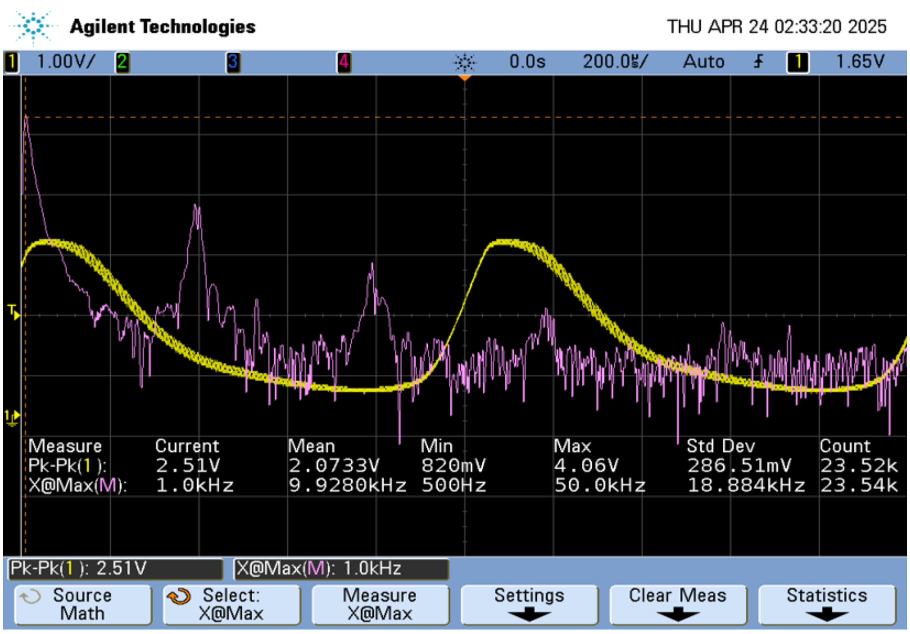

Figure 24: Measured speaker output (TP17) showing final amplified tone.

The speaker output waveform confirms successful amplification and driving of an audible tone, suitable for metal detection feedback.

6 Discussion

In this project, the design was analyzed at three major stages: hand calculations, simulations, and real-world measurements. Hand calculations were used to predict ideal performance, simulations verified practical feasibility, and measurements validated the hardware performance. In this section, the results are compared and discrepancies are discussed.

6.1 Oscillators

Fixed Oscillator:

Stage	Capacitance (nF)	Frequency (kHz)
Calculated	1.0	50
Simulated	1.0	49.8
Measured	1.03	49.9

Table 1: Fixed oscillator comparison.

The values are nearly identical.
Variable Oscillator:

Stage	Capacitance (nF)	Frequency (kHz)
Calculated	1.2	49
Simulated	1.2	49
Measured	1.2	48.9

Table 2: Variable oscillator comparison.

The frequencies are close.

6.2 Mixer and CS Amplifier

Mixer Bias and CS Amplifier Bias:

Node	TP9 (V)	TP10 (V)	TP11 (V)	TP12 (V)
Calculated	1.55	1.2	3.74	4
Simulated	1.3	1.9	4	4.5
Measured	1.51	1.23	3.6	4.1

Table 3: Bias voltages at key test points.

The measured values are reasonably close to calculated ones, with simulated values slightly differing due to different assumptions made during simulation. and also the fact that i had to tune the circuit on the actual board to get as close to the simulated values.

6.3 Filter

Stage	RC Values	Cutoff Frequency (kHz)
Calculated	10k, 1nF	16
Simulated	100, 40nF	39.8
Measured	100, 40nF	40.8

Table 4: Low-pass filter design comparison.

The filter cutoff frequency was adjusted slightly during implementation to improve performance.

6.4 Waveforms

The measurements and simulations of each stage matched the general trends predicted by the hand calculations. Minor variations in frequency and amplitude were observed, along with slight signal clipping at some amplifier outputs. However, the overall operation of the device (including oscillator stability, beat frequency generation, filtering, and amplification) remained consistent and functional.

7 Conclusion

In this project, I successfully designed, simulated, built and tested a fully functional metal detector using fundamental solid-state circuit techniques. The project journey involved a deep integration of theoretical analysis, simulation validation, practical PCB implementation, and experimental tuning.

The operating principle was based on detecting the frequency shift caused by the interaction between a variable LC oscillator and nearby metallic objects. Using the relationship:

$$f_{\text{res}} = \frac{1}{2\pi\sqrt{LC}}$$

I designed two oscillators — one fixed and one variable. When a metallic object approaches the variable inductor, eddy currents are induced according to Faraday's Law and Lenz's Law, altering the inductance and causing a shift in oscillation frequency. This shift is detected by feeding both oscillators into a mixer circuit, generating sum and difference frequencies according to:

$$f_{\text{out}} = |f_{\text{variable}} - f_{\text{fixed}}|$$

By isolating the low-frequency difference component through low-pass filtering, and amplifying it through cascaded amplification stages, an audible signal corresponding to the presence of metal was successfully produced.

Hand Calculations:
Hand calculations were first performed to estimate key operating points, such as oscillator frequencies, bias voltages, differential pair currents, amplifier gains, and filter cutoff frequencies. These calculations established solid design targets but included built-in margins to account for second-order real-world effects.

Simulation Verification:
LTspice simulations were used extensively to verify circuit functionality under ideal conditions. Simulated oscillator frequencies (49–50 kHz), mixer outputs, amplifier responses, and low-pass filter behavior matched theoretical expectations. The simulation step provided crucial insight into nonlinearities, stability, and gain behaviors before hardware implementation.

PCB Implementation:
The circuit was implemented on a carefully designed printed circuit board (PCB) using Altium Designer. Layout strategies emphasized minimizing noise, maintaining signal integrity, and ensuring compact routing. Test points were placed to facilitate in-lab probing and debugging. Despite best practices, unavoidable layout parasitics and slight variations in component values introduced small shifts from the theoretical design.

Measurement and Tuning:
During hardware testing, measured values showed minor deviations from calculated and simulated results. Oscillator frequencies, bias voltages, and gains were all very close but not identical to initial targets. These discrepancies were mainly due to parasitic capacitance, threshold voltage variations among MOSFETs, and PCB trace effects. Through minor resistor and capacitor adjustments on the board, all circuits were tuned to restore intended behavior and maximize performance.

System Performance:
The fixed and variable oscillators achieved stable outputs near 50 kHz. The mixer correctly produced a beat frequency around 1 kHz when metal objects were introduced near the sensing coil. After low-pass filtering, the output was clean, and the final amplifier stages successfully drove an audible tone to the speaker. Overall, the metal detector demonstrated great sensitivity and reliable operation.

Difficulties and Lessons Learned:
One of the main challenges during the project was tuning the circuit on the physical PCB to overcome second-order effects such as parasitic capacitances and threshold voltage variations. Additionally, ensuring oscillator startup and stable mixing required careful adjustment. Through this experience, I learned the importance of bridging theoretical design with practical implementation, and the necessity of empirical adjustments during testing.

Future Improvements:
To further improve the design, adding automatic calibration or more robust filter stages could enhance sensitivity and reduce noise. Advanced layout techniques, such as careful ground shielding and separation of analog/digital sections, would also improve circuit stability and performance.